attributed to the fact that in the AB(edta) family the long-range ordering, if any, occurs at very low temperature, below 1 K. In this temperature range, only the ground Kramers doublet for Co(II) is thermally populated, and the Co(II)–Cu(II) intrachain interaction involving effective spins $^1/_2$ leads to a nonmagnetic ground state. In our case, both intra- and interchain interactions are much more pronounced, so that it is no longer possible to ignore the population of local excited states for Co(II). In other terms, treating Co(II) as an effective spin $^1/_2$ is no longer a good approximation.

To take into account the orbital degeneracy of cobalt(II) and iron(II), we have introduced a branch chain model with z–z interactions between nearest-neighbor local spins S_A and S_B along the chain, and an anisotropic coupling between local spin S_A and local angular momentum L_A along each branch. The intrinsic limit of this model arises from the fact that the magnetic field is assumed to be applied along the z quantization axis; otherwise, the derivation of the thermal properties would not be feasible. This model allows us to reproduce fairly well the magnetic properties of the CoCu and FeCu compounds in the temperature range where the three-dimensional effects may be ignored. Our model has also been tested in the simple case where S_B is zero, B being Ni(II) in a square-planar environment. The rather large values of the intrachain interaction parameters in ACu chain compounds with A = Mn, Fe, Co, and Cu confirm, if it was still necessary, the remarkable ability of conjugated bisbidentate bridging ligands like oxamato to transmit the electronic effects between magnetic centers far apart from each other. The A···Cu separation through the oxamato bridge is indeed about 5.4 Å.

Since the branch chain model is novel, at least in the context of the ferrimagnetic chains, it seems to us interesting to sum up briefly the various models proposed so far to interpret the magnetic properties of ferrimagnetic chains.

(i) Chronologically, the first model is that of $(AB)_N$ ring chains of increasing size, the local spins S_A and S_B being explicitely treated as quantum spins.[2,9,24] The only limitation of this model is the storage capacity of the available computers.

(ii) When both S_A and S_B are large enough, they can be treated as classical spins. An approach of this kind has been developed. This approach leads to an analytical expression for the magnetic susceptibility.[25]

(iii) A classical–quantum model has also been proposed.[26,27] This model, valid when one of the two local spins is large and the other one small, has been applied to the Mn(II)Cu(II) chains.[3,7,8] It has recently been extended to the case of the alternating bimetallic chains.[15,18]

(iv) The anisotropic Ising-type chain has also been investigated for S_A ranging from $^1/_2$ to infinite, S_B remaining equal to $^1/_2$.[28,29] One of the striking results is the occurrence of a compensation temperature, similar to that of three-dimensional ferrimagnets, for a critical ratio between local magnetic momentums g_AS_A and g_BS_B.

(v) The models mentioned above are not valid a priori when at least one of the magnetic centers, e.g., A, is orbitally degenerate. If the orbital degeneracy leads to a ground Kramers doublet, the actual spin S_A of the orbitally degenerate ion may be replaced by an effective spin $^1/_2$. Such an approximation is restricted to the case where the interaction parameter is very small with respect to the energy gap between the ground Kramers doublet and the first excited state. The intrachain interaction may then be considered as of the Ising-type, and model iv becomes relevant.

(vi) Finally, the model developed in this paper is valid for any situation of orbital degeneracy, whatever the magnitude of the intrachain interaction.

To finish with, it is worth mentioning that the application of the branch chain model to the case of bimetallic chains involving an orbital degeneracy is an extension of a work carried by one of us on exotic magnetic systems.[30,31]

Acknowledgment. We express our deepest gratitude to the Société Nationale Elf Aquitaine, which has financially supported this work and offered a research grant to K.N.

Supplementary Material Available: A table of the T, T_1, and T_2 matrices for the CoCu chain compound (3 pages). Ordering information is given on any current masthead page.

(25) Drillon, M.; Coronado, E.; Beltran, D.; Georges, R. *Chem. Phys.* **1983**, *79*, 449.

(26) Seiden, J. *J. Phys., Lett.* **1983**, *44*, L947.

(27) Verdaguer, M.; Gleizes, A.; Renard, J. P.; Seiden, J. *Phys. Rev.* **1984**, *B29*, 5144.

(28) Curely, J.; Georges, R.; Drillon, M. *Phys. Rev.* **1986**, *B33*, 6243.

(29) Georges, R.; Curely, J.; Drillon, J. *Appl. Phys.* **1985**, *58*, 914.

(30) Drillon, M.; Coronado, E.; Belaiche, M.; Carlin, R. L. *J. Appl. Phys.* **1988**, *63*, 3551.

(31) Drillon, M.; Belaiche, M.; Heintz, J. M.; Villeneuve, G.; Boukhari, A.; Aride, J. In *Organic and Inorganic Low-Dimensional Crystalline Materials*; Delhaes, P., Drillon, M., Eds.; NATO ASI Series 168; Plenum: New York, 1987; p 421.

Contribution from the Department of Chemistry, Gorlaeus Laboratories, Leiden University, P.O. Box 9502, 2300 RA Leiden, The Netherlands

Synthesis, Structure, and Properties of a Trinuclear and a Mononuclear Nickel(II) Complex of *N*,*N*′-Dimethyl-*N*,*N*′-bis(β-mercaptoethyl)ethylenediamine

Mary A. Turner, Willem L. Driessen, and Jan Reedijk*

Received January 24, 1990

The N_2S_2 ligand *N*,*N*′-dimethyl-*N*,*N*′-bis(β-mercaptoethyl)ethylenediamine, H_2L, reacts with $NiCl_2{\cdot}6H_2O$ in methanol solution to yield a trinuclear species of stoichiometry $[Ni_3L_2]Cl_2{\cdot}2H_2O$. This compound crystallizes in the monoclinic space group $P2_1/n$ with a = 19.917 (7) Å, b = 5.453 (3) Å, c = 13.508 (6) Å, β = 100.81 (4)°, and Z = 2. The trinuclear unit consists of two pseudosquare-planar terminal NiN_2S_2 environments arranged in a chair conformation about a central NiS_4 plane, with the central nickel occupying a crystallographic inversion center. A dihedral angle of 107.84 (7)° exists between nickel planes unrelated by symmetry. Ni–N distances are 1.938 (4) and 1.951 (3) Å, Ni–S distances in the NiN_2S_2 environment are 2.144 (1) and 2.160 (1) Å, and Ni–S distances of the NiS_4 center are 2.219 (1) and 2.216 (1) Å. The same ligand, under aprotic conditions, reacts with bis(acetylacetonato)nickel(II) to give a neutral mononuclear [NiL] unit with an NiN_2S_2 chromophore. The trinuclear and mononuclear species are compared with respect to their syntheses and NMR and electronic absorption spectra.

Introduction

The partial characterization of the nickel site in bacterial hydrogenases has prompted efforts to model the nickel environment in these proteins.[1-8] Features of the enzyme active site typically taken as modeling criteria are ligation of a Ni(III) center by anionic sulfur ligands—evidence for which has been observed in

(1) Kruger, H.-J.; Holm, R. H. *Inorg. Chem.* **1989**, *28*, 1148.

0020-1669/90/1329-3331$02.50/0

EPR spectra and EXAFS of enzyme preparations.[9-12] The actual number of sulfur donors present is as yet uncertain. Current estimates suggest three to six sulfur donors with the possibility of nitrogen or oxygen donor ligands making up the complement of a potentially pseudooctahedral nickel coordination sphere.[12] ESEEM data from measurements of oxidized *Desulfovibrio gigas* hydrogenase show evidence of superhyperfine interactions of the unpaired Ni(III) electron with a nearby ^{14}N nucleus. Furthermore, it has been suggested, on the basis of the estimated electric field gradient of this ^{14}N nucleus, that a weak interaction with an imidazole ligand is possible.[13]

Limited information as to coordination geometry of the nickel site is available from EPR and MCD spectra of oxidized enzymes. These techniques indicate a low-spin state of Ni(III), although it becomes difficult to apply fundamental EPR concepts based on the more regular geometries of simple compounds to interpret the probable highly distorted coordination environment of nickel in the enzyme. Thus "rhombic" EPR spectra give little detailed information about the coordination sphere. The conclusion drawn as a result of MCD studies was that the nickel(II) thiolate center of hydrogenase was diamagnetic, indicating square-planar, square-pyramidal, or strongly axially distorted octahedral geometry.[14] Finally, EPR studies of ^{13}CO-treated *Chromatium vinosum* hydrogenase have shown that nickel is the CO-binding site.[12] This suggests a coordinatively unsaturated metal ion in the active enzyme or coordination of a weaker ligand that can be replaced by carbon monoxide (or H_2). A vacant site also fits with hypotheses of enzyme reaction mechanisms.[12]

In light of available evidence concerning the environment of nickel in hydrogenases, we have incorporated the N_2S_2 chelate ligand *N,N'*-dimethyl-*N,N'*-bis(β-mercaptoethyl)ethylenediamine (H_2L) to initiate our study of models of the enzyme active site.

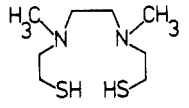

H_2L

The ligand offers two anionic sulfur donor sites and has the potential to impose steric strain in a tetragonally coordinated nickel complex.

The use of the H_2L system has also allowed us to test certain hypotheses concerning nickel thiolate chemistry. For example, a difficulty associated with many metal thiolates, and in particular nickel, is that complexes have a tendency to oligomerize under certain reaction conditions. It has been pointed out[1] that protic media may play a role in the extent of product oligomerization. We have isolated and characterized both mononuclear and trinuclear species starting from H_2L under different reaction conditions, and the implications of this will also be discussed.

Table I. Summary of X-ray Data Collection and Refinement for $[Ni_3L_2]Cl_2 \cdot 4H_2O$

chem formula	$C_{16}H_{44}Cl_2N_4Ni_3S_4O_4$
mol wt	731.82
cryst syst	monoclinic
a, Å	19.917 (7)
b, Å	5.453 (3)
c, Å	13.508 (6)
β, deg	100.81 (4)
V, Å^3	1440.9 (1)
space group	$P2_1/n$ (No. 14)
Z	2
density (calc), g cm^{-3}	1.68
μ, cm^{-1}	24.32
h range	−32 to +32
k range	0 to +8
l range	0 to +21
radiation (λ, Å)	Mo Kα (0.71073)
T, °C	21
R, R_w	0.050, 0.054
goodness of fit (*S*)	2.20
F(000)	764

Experimental Section

Preparation of Compounds. The ligand, H_2L, was prepared through the known mercaptoethylation reaction of *N,N'*-dimethylethylenediamine with ethylene sulfide in anhydrous toluene.[15] *Note of Caution*: Contact of the ligand or its vapor with skin should be avoided, as severe allergic reactions have been reported.[16] Starting materials were obtained from Aldrich. Dried solvents were degassed on standard Schlenk equipment prior to use. Nickel analyses were carried out by standard EDTA titrations.[17] C, H, and N analyses were performed by University College, Dublin.

$[Ni_3L_2]Cl_2 \cdot 4H_2O$. A solution of 2.01 g (0.0097 mol) of H_2L in 10 mL of ethanol was added to a stirred solution (30 mL) of 3.45 g of $NiCl_2 \cdot 6H_2O$ (0.0145 mol). The solution, which became dark red immediately upon ligand addition, was stirred for 4 h, the solvent volume was reduced to 10 mL, and the dark red microcrystalline product was separated by filtration. A second crop of product was obtained after further evaporation of the filtrate. The product was stable in air but extremely hygroscopic. Recrystallization from methanol yielded 64% of pure product. Anal. Calcd for $C_{16}H_{36}Cl_2N_4Ni_3S_4 \cdot 4H_2O$: C, 26.26; H, 6.06; N, 7.66; Ni 24.06. Found: C, 25.7; H, 5.8; N, 7.5; Ni, 21.2. IR: 3410, 1625, 1468, 1290, 1237, 1200, 1060, 970, 770 cm^{-1}. μ: 3.12 (MeOD), 1.61 μ_B (solid). *m/z*: 589, corresponding to the cationic unit.

[NiL]. The ligand, H_2L (3.49 g, 0.0168 mol), was reacted with sodium ethoxide (0.77 g, 0.033 mol of Na) in 45 mL of ethanol. The solvent was removed, and the residue was dissolved in 20 mL of acetonitrile. A solution containing 3 g (0.01 mol) of bis(acetylacetonato)nickel(II) in 30 mL of acetonitrile was added to produce a dark red solution, with a quantity of red precipitate appearing by the end of the metal addition. The reaction mixture stood at room temperature overnight before filtering to afford a mixture of the red mononuclear product and precipitated sodium acetylacetonate. Purification was accomplished by extraction of the nickel compound with 20 mL of chloroform followed by reprecipitation with hexanes. Recrystallization of the pink material in chloroform/hexanes (4:1 v/v) produced small hygroscopic crystals (34% yield) that powdered during filtration as a result of solvent loss. Anal. Calcd for $C_8H_{18}N_2NiS_2 \cdot {}^2/_3H_2O$: C, 34.65; H, 6.98; N, 10.10, Ni; 21.18. Found: C, 34.7; H, 6.5; N, 9.8; Ni, 20.76. IR: 2950, 1479, 1294, 1228, 1190, 1042, 939, 776, 388 cm^{-1}. μ: 2.46 μ_B ($CDCl_3$).

X-ray Structural Determination of $[Ni_3L_2]Cl_2 \cdot 4H_2O$. Dark red single crystals of $[Ni_3L_2]Cl_2 \cdot 4H_2O$ were obtained through slow evaporation of a methanol solution. The crystal used in X-ray work was a 0.35 × 0.25 × 0.45 mm^3 rod that was mounted in a glass capillary, and the crystal system was determined by preliminary Weissenberg photography. Data collection was carried out by an ω–2θ scan on an Enraf-Nonius CAD-4 diffractometer with use of graphite-monochromatized Mo Kα radiation. Unit cell parameters and final orientation matrices were determined by

(2) Rosenfield, S. G.; Wong, M. L. Y.; Stephan, D. W.; Mascharak, P. K. *Inorg. Chem.* **1987**, *26*, 4119.
(3) Rosenfield, S. G.; Armstrong, W. H.; Mascharak, P. K. *Inorg. Chem.* **1986**, *25*, 3014.
(4) Kumar, M.; Day, R. O.; Colpas, G. J.; Maroney, M. J. *J. Am. Chem. Soc.* **1989**, *111*, 5974.
(5) Handa, M.; Mikuriya, M.; Okawa, H.; Kida, S. *Chem. Lett.* **1988**, 1555.
(6) Tremel, W.; Kriege, M.; Krebs, B.; Henkel, G. *Inorg. Chem.* **1988**, *27*, 3886.
(7) Kruger, H.-J.; Holm, R. H. *Inorg. Chem.* **1987**, *26*, 3645.
(8) Nicholson, J. R.; Christou, G.; Huffman, J. C.; Folting, K. *Polyhedron* **1987**, *6*, 863.
(9) Lindahl, P. A.; Kojima, N.; Hausinger, R. P.; Fox, J. A.; Teo, B. K.; Walsh, C. T.; Orme-Johnson, W. H. *J. Am. Chem. Soc.* **1984**, *106*, 3062.
(10) Scott, R. A.; Wallin, S. A.; Czechowski, M.; DerVartanian, D. V.; LeGall, J.; Peck, H. D.; Moura, I. J. Am. Chem. Soc. **1984**, *106*, 6864.
(11) Eidsness, M. K.; Sullivan, R. J.; Scott, R. A. Electronic and Molecular Structure of Biological Nickel as Studied by X-ray Absorption Spectroscopy. In *The Bioinorganic Chemistry of Nickel*; Lancaster, J. R., Ed.; VCH Publishers Inc.: New York, 1988; p 73.
(12) Cammack, R. *Adv. Inorg. Chem.* **1988**, *32*, 297.
(13) Chapman, A.; Cammack, R.; Hatchikian, C. E.; McCracken, J.; Peisach, J. *FEBS Lett.* **1988**, *242*, 134.
(14) Kowal, A. T.; Zambrano, I. C.; Moura, I.; Moura, J. J. G.; LeGall, J.; Johnson, M. K. *Inorg. Chem.* **1988**, *27*, 1162.
(15) Corbin, J. L.; Miller, K. F.; Paryadath, N.; Wherland, S.; Bruce, A. E. *Inorg. Chim. Acta* **1984**, *90*, 41.
(16) Hu, W. J.; Barton, D.; Lippard, S. J. *J. Am. Chem. Soc.* **1973**, *95*, 1170.
(17) Vogel, A. J. *Quantitative Inorganic Analysis*; Longmans, Green and Co.: London, 1959.

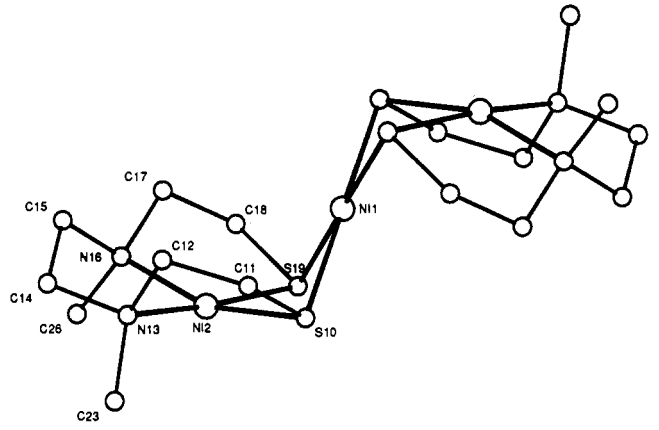

Figure 1. The $[Ni_3L_2]^{2+}$ cation showing the atom labeling and the chair structure of the trinuclear unit. Hydrogen atoms have been omitted for clarity.

least-squares refinement of 25 reflections with $3.37° < \theta < 19.94°$. Details of scan rate and background estimation are described elsewhere.[18] Standard reflections measured every 5400 s showed no significant changes in intensity. Out of 6870 independent reflections obtained, 3490 were regarded as significant with $I > 2\sigma(I)$ and were subsequently used in the refinement. The intensity data were treated for Lorentz and polarization effects. Absorption correction was not applied.

Positions of the Ni atoms did not follow unequivocally from a three-dimensional Patterson synthesis; thus the direct-methods program MULTAN was used to solve the phase problem.[19] Atomic scattering factors were taken from literature tabulations.[20] The positions of non-hydrogen atoms of the cation were determined with use of the program AUTOFOUR.[21] Block-matrix difference syntheses revealed all other non-hydrogen atoms. The temperature factors of the non-hydrogen atoms were refined anisotropically. All hydrogen atoms (except those associated with a disordered water molecule) were located from difference maps and refined coupled to their parent atoms to a final thermal temperature parameter of 4.28 Å^2. In an attempt to sort out the disorder of O5, belonging to lattice water, site occupation of the isotropic atom was refined to two positions at roughly 40% (O5A) and 60% (O5B) occupancy, each having thermal temperature factors fixed at 6.2 Å^2. Further refinements by full-matrix least-squares, minimizing the function $\Sigma w(|F_o| - |F_c|)^2$ where $w = (\sigma^2(F))^{-1}$ was terminated when the maximum shift/error was <0.3. Other details of data collection and structure refinement are given in Table I.

Other Physical Measurements. Solution electronic spectra in the range 10 000–3333 cm^{-1} were recorded at room temperature on a Perkin-Elmer 330 spectrometer, and solid-state spectra, on the same instrument (33 000–5000 cm^{-1}) fitted with a reflectance attachment with $BaSO_4$ as reference material. Standard ^{1}H NMR spectra were measured on a JEOL 200 spectrometer, and a Bruker WM-300 instrument was used for 2D COSY and spin magnetization transfer experiments. Infrared spectra from 4000 to 200 cm^{-1} were recorded as KBr pellets on a Perkin-Elmer 580 spectrometer. Plasma desorption mass spectroscopy was performed on a BIO-ION 20 instrument. Magnetic susceptibility measurements were done on a Faraday balance calibrated with $CoHg(SCN)_4$. Solution magnetic susceptibility was measured in MeOD or $CDCl_3$ (solutions were approximately 0.01 M in Ni) according to the Evans method.[22,23]

Results and Discussion

General Comments. It has been suggested[2] that, during the formation of the trinuclear β-mercaptopropionato complex, in situ generation of mononuclear units first occurs, followed by coordination of two such units to Ni^{2+}. With H_2L as the ligand in protic media, the charged trinuclear species is apparently stabilized and is the only product isolated even from reaction mixtures with 1:1 nickel:ligand stoichiometry. Under dry, aprotic conditions, the neutral mononuclear complex is produced and, once isolated, is also stable in protic media in the absence of excess nickel. Addition of $NiCl_2$ to ethanolic solutions of [NiL] results in quantitative production of $[Ni_3L_2]Cl_2·4H_2O$, while no trinuclear species is observed when excess bis(acetylacetonato)nickel(II) is added to solutions of [NiL] in dry acetonitrile.

Crystal Structure of $[Ni_3L_2]Cl_2·4H_2O$. The structure of the $[Ni_3L_2]^{2+}$ cation is shown in Figure 1. Atomic positional parameters are listed in Table II, and selected interatomic distances and angles are given in Table III. The overall geometry of the trinuclear cation is described as a chair consisting of three pseudosquare planes. The dihedral angle formed between these planes is 107.84 (7)°. This angle is similar to that in the related tetrakis((β-mercaptoethyl)amine)trinickel(II) structure (109°)[24] and somewhat smaller than those found in the anionic O,S- and S,S-chelating species tetrakis(2-mercaptopropionato)trinickelate(II), $[Ni_3(CH_3CH(S)CO_2)_4]^{2-}$ (115°),[2] and tetrakis(ethanedithiolato)trinickelate(II), $[Ni_3(SCH_2CH_2S)_4]^{2-}$ (116.8°).[8] Associated with the dihedral angles between the nickel planes are the degree of folding along the S···S vector and the distance of approach of the nickel centers. The Ni···Ni distance in the present structure is 2.748 (1) Å and is marginally longer than that in the (β-mercaptoethyl)amine structure (2.733 (7) Å). MO calculations using data from the latter structure suggest that such a distance is indicative of a Ni–Ni interaction and may contribute to the

Table II. Atomic Coordinates (×10^5 for Ni, Cl, and S; ×10^4 for C, N, and O) and Isotropic Temperature Factors for the Non-Hydrogen atoms of $[Ni_3L_2]Cl_2·4H_2O$

atom	x	y	z	B_{eq}, Å^2 × 10^2
Ni1	100000	0	100000	172 (2)
Ni2	95074 (3)	11814 (11)	117078 (4)	164 (1)
Cl3	36048 (7)	11916 (27)	97985 (9)	366 (3)
O4	2179 (2)	1123 (9)	4890 (4)	563 (3)
O5A	2658 (7)	−60 (46)	3135 (11)	620[a]
O5B	2724 (5)	1174 (31)	2998 (7)	620[a]
S10	89902 (5)	15043 (18)	101583 (7)	203 (2)
C11	8373 (2)	−962 (9)	10207 (3)	269 (11)
C12	8509 (3)	−2243 (9)	11216 (4)	273 (11)
N13	8716 (2)	−446 (7)	12049 (3)	219 (9)
C14	8955 (3)	−1690 (9)	13041 (4)	304 (13)
C15	9707 (3)	−2334 (9)	13154 (4)	311 (12)
N16	10078 (2)	−114 (7)	12928 (2)	214 (8)
C17	10743 (3)	−796 (9)	12649 (3)	289 (12)
C18	11034 (2)	1316 (11)	12172 (3)	319 (12)
S19	103765 (5)	27030 (18)	112016 (7)	219 (3)
C23	8132 (3)	1184 (11)	12137 (4)	312 (12)
C26	10198 (3)	1531 (9)	13819 (3)	287 (12)

[a] See text for this value.

Table III. Interatomic Distances (Å) and Angles (deg) for $[Ni_3L_2]Cl_2·4H_2O$

Ni1–S10	2.219 (1)	Ni1–S19	2.216 (1)	Ni2–S10	2.160 (1)
Ni2–N13	1.938 (4)	Ni2–N16	1.951 (3)	Ni2–S19	2.144 (1)
S10–C11	1.832 (5)	C11–C12	1.511 (7)	C12–N13	1.490 (6)
N13–C23	1.487 (6)	N13–C14	1.498 (6)	C14–C15	1.519 (7)
C15–N16	1.480 (6)	N16–C26	1.485 (5)	N16–C17	1.489 (5)
C17–C18	1.489 (7)	C18–S19	1.833 (5)		
Ni1···Ni2	2.748 (1)	S10···S19	3.390 (3)		

S10–Ni1–S19	82.64 (4)	S10–Ni2–N13	90.4 (1)
S19–Ni2–N16	160.9 (1)	S10–Ni2–S19	85.77 (4)
N13–Ni2–N16	90.3 (2)	N13–Ni2–S19	173.9 (1)
N16–Ni2–S19	91.8 (1)	Ni1–S10–Ni2	77.71 (4)
Ni1–S10–C11	111.0 (2)	Ni2–S10–C11	96.1 (1)
S10–C11–C12	111.3 (3)	C11–C12–N13	110.8 (4)
C12–N13–C23	110.1 (4)	C12–N13–C14	112.0 (4)
N13–C14–C15	109.6 (3)	C14–C15–N16	108.2 (4)
C15–N16–C26	109.7 (3)	C15–N16–C17	110.5 (4)
N16–C17–C18	110.7 (4)	C17–C18–S19	110.2 (3)
C18–S19–Ni2	97.1 (2)	C18–S19–Ni1	110.3 (2)
Ni2–S19–Ni1	78.10 (4)		

(18) Schilstra, M. J.; Birker, P. J. M. W. L.; Verschoor, G. C.; Reedijk, J. *Inorg. Chem.* **1982**, *21*, 2637.
(19) Germain, G.; Main, P.; Woolfson, M. M. *Acta Crystallogr. Sect. B.* **1970**, *B26*, 274.
(20) Kinneging, A. J.; de Graaff, R. A. G. *J. Appl. Crystallogr.* **1984**, *17*, 364.
(21) Cromer, D. T.; Waber, J. T. *International Tables for Xray Crystallography*; Kynoch Press: Birmingham, U.K., 1974; Vol. IV.
(22) Evans, D. F. *J. Chem. Soc.* **1959**, 2003.
(23) Loliger, J.; Scheffold, R. *J. Chem. Educ.* **1972**, *49*, 646.

Table IV. ^1H and ^{13}C NMR Peaks and Assignments for $[Ni_3L_2]Cl_2 \cdot 4H_2O$ and [NiL] in MeOD

	assgnt	peak positions, ppm[a]	
		$[Ni_3L_2]^{2+}$	[NiL]
^{13}C	C11 (C18)	31.95	27.79
	C23 (C26)	42.28	43.62
	C14 (C15)	58.96	61.22
	C12 (C17)	64.51	65.67
^1H	H11 (H18)	3.14, 4.10 m, br	2.31, 2.66 m, br
	H23 (H26)	3.37 s	2.89 s
	H12 (H17)	4.24, 4.51 m[b]	2.66, 3.06 m
	H14 (H15)	3.97, 4.46 m	2.45, 3.37 m

[a] ppm values are reported relative to TMS (intenal). m = multiplet; br = broad; s = singlet. [b] J_m = 9 Hz.

stability of the trinuclear arrangement.[24]

The central nickel atom is located on a crystallographic inversion center; thus the NiS_4 environment is rigorously planar as required by symmetry. Each Ni2 atom is bound to two nitrogen atoms and two sulfur atoms; Ni–S bond lengths are identical with those reported for the tetrakis((β-mercaptoethyl)amine)trinickel structure, while Ni-N distances are marginally longer in comparison.[24] Whereas (β-mercaptoethyl)amine is didentate and two ligands are required to form a square-planar nickel complex, L is tetradentate. The implications of this distinction are manifest in a comparison of geometries about the Ni2 center. The terminal N13–Ni2-N16 angles are constrained in the present structure to the square 90.3 (2)°, whereas the corresponding angle in the (β-mercaptoethyl)amine structure is 96.1 (3)°.[24] The only angle that deviates significantly from the square is S10–Ni2–S19 (85.77 (4)°) and is the only angle not constrained by the ligand. Such a value for this angle is, however, typical in trinuclear structures and has been explained on the basis of an interaction between the sulfur atoms located, for example, 2.89 (1) Å apart in the (β-mercaptoethyl)amine structure. This distance is much longer in the present structure (3.390 (3) Å), although it is less than the sum of the van der Waals radii (3.60 Å)[25] and thus may be indicative of an attractive interaction. The effect of chelate restrictions imposed by L is apparent in the distinctly nonlinear S10–Ni2–N16 (160.9 (1)°) and S19–Ni2–N13 (173.9 (1)°) angles. As a result, the planarity of the Ni2 site is disturbed such that the Ni2 sits 0.217 (2) Å out of the N_2S_2 plane.

Packing in the structure occurs in layers of trinuclear units with the chair axis roughly parallel to the body diagonal. The space between the cationic layers is occupied by the "anionic" hydrogen-bonded layer. The shortest contact between nickel atoms of the cationic layer and atoms in the hydrogen-bonded layer involve chlorine atoms at a Ni2···Cl3 distance of 5.053 (1) Å. Water molecules and chloride ions are mutually involved in hydrogen bonding such that the chloride accepts hydrogen bonds from two O4 water atoms located at distances of 3.176 (4) and 3.240 (4) Å with an associated O4···Cl3···O4′ (thus Cl3···O4···Cl3′) angle of 116.4 (4)°. The water molecules are also hydrogen-bonded to each other with an O4···O5A distance of 2.792 (6) Å. The disordered oxygen atoms O5A and O5B appear to be a result of the possibility of hydrogen-bond formation with either O4 or itself.

NMR Spectra. The stability and diamagnetism of the planar nickel(II) complexes have allowed their characterization by ^1H and ^{13}C NMR spectroscopies. A slight degree of paramagnetism observed in solution may be attributed to small fluctuations at the nickel center toward square-pyramidal gometry. However, also a tetrahedral ($S = 1$) ⇄ planar ($S = 0$) equilibrium of the central fragment could contribute to this paramagnetic contribution.[3,14] A detailed study of such equilibria would require solid-state and solution magnetic measurements over a wide temperature range. Given the fact that two chemically distinct Ni sites occur, this was not undertaken.

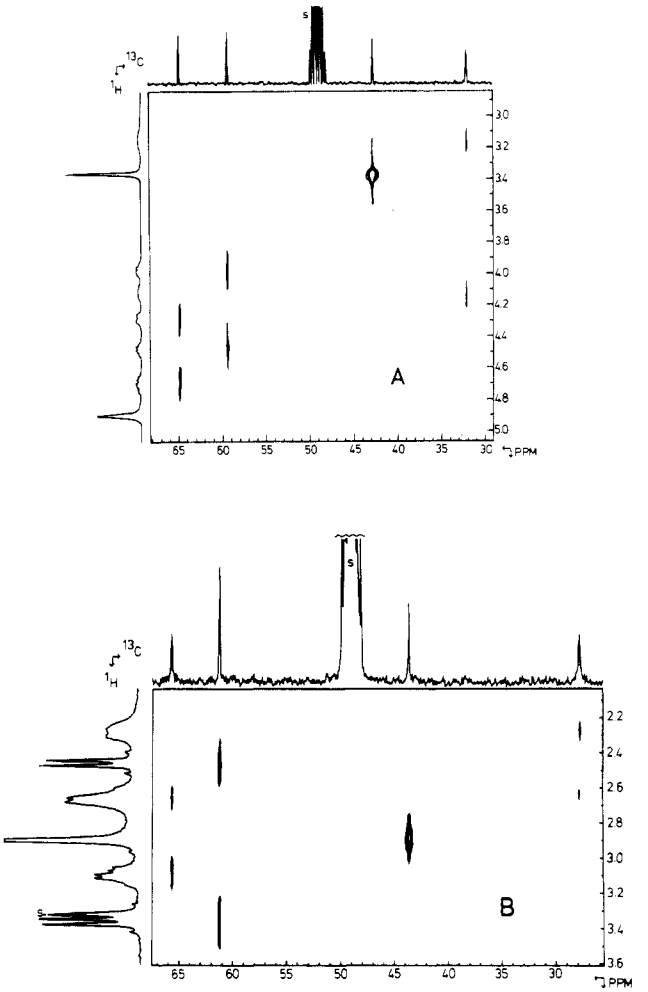

Figure 2. ^{13}C–^1H COSY 2D NMR spectra in methanol solution for (A) $[Ni_3L_2]^{2+}$ and (B) [NiL]. Peaks resulting from solvent resonances are denoted by s.

Lists of NMR peaks and assignments are found in Table IV. Spectra are simplified by apparent mirror symmetry of the molecules in solution. Assignments for both ^{13}C and ^1H spectra were based on ^{13}C–^1H 2D NMR results illustrated in Figure 2 as well as spin magnetization transfer experiments. A notable comparison in ^{13}C spectra of [NiL] and $[Ni_3L_2]Cl_2 \cdot 4H_2O$ is the 4 ppm downfield shift in the resonance of the β-carbon, C11 (C18), when the sulfur of the mononuclear unit coordinates to another nickel atom. Such a downfield shift is also observed for the β-C resonance when a second $Pt(dien)^{2+}$ moiety binds to the sulfur of a Pt(dien)–glutathione complex.[26] The positions of other carbon resonances change only slightly from mononuclear to trinuclear species. Overall appearance of proton spectra of the [NiL] compared to $[Ni_3L_2]Cl_2 \cdot 4H_2O$ is characterized by a downfield shift of the proton resonances, which may be related to inductive effects related to comparison of neutral and cationic species. It is also notable that, in ^1H NMR spectra of both [NiL] and $[Ni_3L_2]Cl_2 \cdot 4H_2O$, sharper peaks are observed for protons located on carbons adjacent to nitrogen atoms, while those arising from protons on carbons adjacent to sulfur are broader. This is tentatively attributed to the relative rigidity of the ligand backbone in proximity to the coordinated nitrogen atoms and the relative mobility of this backbone near the sulfur atoms[18]—even when sulfur acts as a bridge between two nickel atoms in the case of the trinuclear compound. Large chemical shift differences in axial and equatorial proton resonances are apparent especially in the

(24) Wei, C. H.; Dahl, L. F. *Inorg. Chem.* **1970**, *9*, 1878.
(25) Bondi, A. *J. Phys. Chem.* **1964**, *68*, 441.
(26) (a) Lempers, E. L. M.; Inagaki, K.; Reedijk, J. *Inorg. Chim. Acta* **1988**, *152*, 201. (b) Lempers, E. L. M.; Reedijk, J. *Inorg. Chem.* **1990**, *29*, 217.

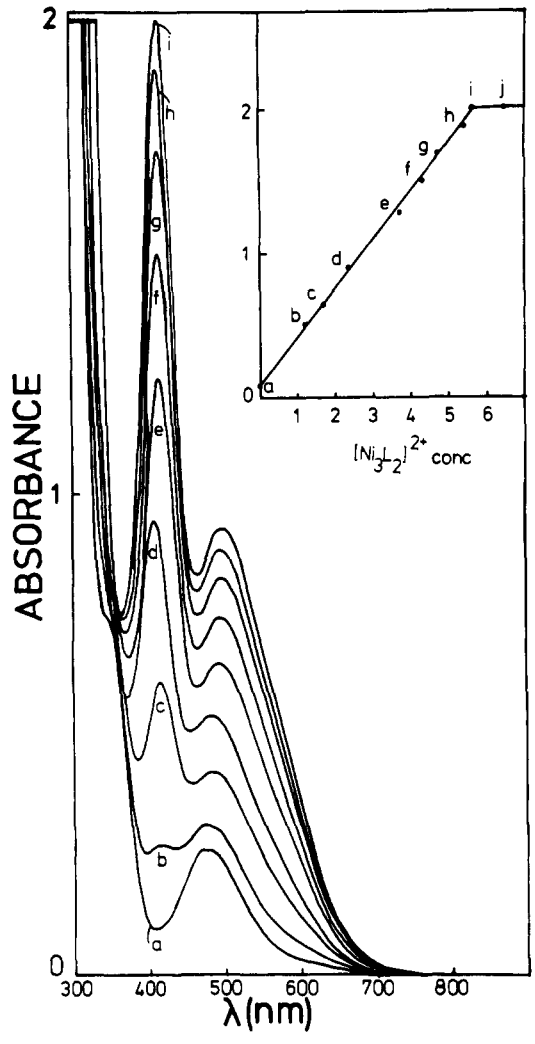

Figure 3. Spectral changes during the course of $NiCl_2$ addition to [NiL] in ethanol solution: (a) initial [NiL] spectrum (1.5×10^{-3} M); (b–j) resulting spectra after incremental addition of 0.25-mL aliquots of 1.4×10^{-3} M $NiCl_2$ solution. Inset: Plot of absorbance of the 410-nm peak with increasing $[Ni_3L_2]^{2+}$ concentration. $[Ni_3L_2]^{2+}$ concentration was based on amount of $NiCl_2$ added, assuming quantitative reaction with [NiL].

case of the trinuclear species, where proximity to the central filled d_{z^2} orbital of Ni1 is expected to have a shielding effect on the axial protons of C11 (C18) and C14 (C15).

Electronic Absorption Spectra. A list of absorption maxima for the complexes is given in Table V. Electronic absorption spectroscopy has proven very useful in distinguishing between trinuclear and mononuclear species and has been used to monitor

Table V. Electronic Absorption Data for $[Ni_3L_2]Cl_2 \cdot 4H_2O$ and [NiL]

	peak positions, nm[a]	
solvent	$[Ni_3L_2]$	[NiL]
ethanol	411 (4450), 496 sh (2250)	338 (520), 473 (182)
acetonitrile	410 (2300), 477 sh (1323)	345 (660), 462 (284)
dimethylformamide	404 (1470), 465 sh (1010)	348 (405), 477 (172)
chloroform		344 (830), 476 (350)
solid	304, 334, 479 sh, 581 sh	406, 496, 700 br, sh

[a] Molar absorptivity coefficient (cm^{-1} M^{-1}) in parentheses. sh = shoulder; br = broad.

the titration of the mononuclear complex with $NiCl_2$ in ethanol solution. Results of this titration are shown in Figure 3. The initial spectrum of the mononuclear compound is typical of square-planar d^8 species[27] and consists of a peak at 473 nm assigned to the $^1A_{1g}$–$^1A_{2g}$ transition. A second peak at approximately 338 nm in ethanol solution, assigned to $^1A_{1g}$–$^1B_{2g}$, appears as a shoulder to a high-intensity peak at about 325 nm for which a charge-transfer transition is probably responsible.[27] Upon addition of $NiCl_2$, a new, sharper peak appears at 410 nm. The linear plot of increase of this absorption vs concentration of $NiCl_2$ (see Figure 3, inset) indicates quantitative production of the trinuclear complex until the mononuclear complex is exhausted at a 1:2 $NiCl_2$:[NiL] ratio. The peak at 410 nm is tentatively assigned to the $^1A_{1g}$–$^1A_{2g}$ transition of the NiS_4 chromophore. This peak is also present in spectra of the trinuclear 2-mercaptopropionato species (420 nm in DMF)[2] and of the corresponding ethanedithiolato complex (392 nm in acetonitrile or 424 nm in methanol[8]). This assignment may be justified on the basis of comparison with the spectrum of (1,4,8,11-tetrathiacyclotetradecane)nickel(II), which has a corresponding maximum at 494 nm.[29] Essentially, the central nickel of these trinuclear units may be described as being coordinated by four "thioether-type" donors, with the coordinated thiolates being somewhat stronger ligands than actual thioethers. Appearance of the trinuclear product is associated with a slight shift to lower energy of the NiN_2S_2 $^1A_{1g}$–$^1A_{2g}$ transition.

Acknowledgment. The authors are indebted to the Stichting voor Technische Wetenschappen (STW) and the Netherlands Organization for Scientific Research (NWO) for financial support of this research and a postdoctoral fellowship granted to M.A.T. We thank Dr. S. P. J. Albracht for helpful discussions and Mr. S. Gorter and Dr. R. A. G. de Graaff for assistance with X-ray data collection and processing.

Supplementary Material Available: Tables of anisotropic thermal parameters, hydrogen parameters, interatomic distances, and hydrogen-bond distances (4 pages); a list of structure factors (12 pages). Ordering information is given on any current masthead page.

(27) Lever, A. B. P. *Inorganic Electronic Spectroscopy*, 2nd ed.; Elsevier Science: Amsterdam, 1984.
(28) Yamamura, T.; Miyamae, H.; Katayama, Y.; Sasaki, Y. *Chem. Lett.* **1985**, 269.
(29) Rosen, W.; Busch, D. H. *J. Am. Chem. Soc.* **1969**, *91*, 4694.